2019 American Control Conference (ACC)
Philadelphia, PA, USA, July 10-12, 2019

Stochastic analysis of genetic feedback controllers to reprogram a pluripotency gene regulatory network

Simone Bruno[1] and M. Ali Al-Radhawi[1] and Eduardo D. Sontag[2] and Domitilla Del Vecchio[1]

***Abstract*—Cellular reprogramming is traditionally accomplished through an open loop (OL) control approach, wherein key transcription factors (TFs) are injected in cells to steer the state of the pluripotency (PL) gene regulatory network (GRN), as encoded by TFs concentrations, to the pluripotent state. Due to the OL nature of this approach, the concentration of TFs cannot be accurately controlled. Recently, a closed loop (CL) feedback control strategy was proposed to overcome this problem with promising theoretical results. However, previous analyses of the controller were based on deterministic models. It is well known that cellular systems are characterized by substantial stochasticity, especially when molecules are in low copy number as it is the case in reprogramming problems wherein the gene copy number is usually one or two. Hence, in this paper, we analyze the Chemical Master Equation (CME) for the reaction model of the PL GRN with and without the feedback controller. We computationally and analytically investigate the performance of the controller in biologically relevant parameter regimes where stochastic effects dictate system dynamics. Our results indicate that the feedback control approach still ensures reprogramming even when both the PL GRN and the controller are stochastic.**

I. INTRODUCTION

Cellular reprogramming is an approach to convert a differentiated cell type (such as a fibroblast) to a pluripotent cell type (known as an induced pluripotent stem cell or iPS cell). Human iPS cells, functionally equivalent to embryonic stem cells (ESCs), are the best alternative to ESCs in regenerative medicine, especially for laboratory research, in which the use of ESCs faces ethical and political barriers [1], [2].

The first iPS cell (iPSC) reprogramming approach was proposed by Yamanaka et al. [3], who obtained iPS cells by constant overexpression of four key transcription factors. From a control theoretic point of view, the GRN can be viewed as the plant to be controlled and the overexpression of select TFs can be viewed as a control input. Therefore, current reprogramming approaches can be regarded as OL control.

Several studies have been conducted in order to improve the performance of this reprogramming method ([4], [5]), but its efficiency remains as low as 1% [6], [7]. In a more recent study [1], it has been proposed that the fact that the core PL GRN is a monotone dynamical system ([9]) along with the fact that the target pluripotent (PL) state may not be associated with extremal concentrations of TFs ([1]), may contribute to failure of current reprogramming practices based on OL control. This led a novel feedback control approach to reprogramming ([1]), in which the TFs constant overexpression is replaced by a variable one, implemented by a negative feedback control. This control law can be implemented through a synthetic genetic circuit that can be delivered to the cells through standard infection methods [11]. The proposed approach is theoretically able to reach the desired steady state (SS) as demonstrated through preliminary studies based on ODE models [1].

However, both the plant to be controlled (the PL GRN) and the controller (the synthetic genetic circuit) are realized through chemical reactions, which are inherently stochastic [12], [13], [14]. This is especially the case for differentiation as this is often driven by noise, due, in part, to the combination of low molecular counts and slow promoter kinetics (i.e., when the process of binding and unbinding of TFs to promoters is slow) [15]. In order to determine the extent to which the feedback control approach still ensures to steer the network state to the PL state when stochastic effects are taken into account, in this paper we analyze the performance of the controller with a stochastic model of the CL system in parameter regimes where stochasticity is not negligible. We first consider the limit of slow promoter kinetics, small volume and one copy of each TF's gene. Second, we explore when the promoter kinetics is on the same time scale as protein kinetics, which may be a more realistic assumption for certain applications [16]. Specifically, we simulated the CL system with the Gillespie algorithm ([22]) and compared the results to those obtained using the OL control. For the slow promoter kinetics parameter regime the performance of this reprogramming approach was further evaluated through a recently proposed analytical method [17], based on the systematic application of singular perturbation to the CME [18].

This paper is organized as follows. In Section 2, we describe the PL GRN model and summarize the previous results obtained with the deterministic approach. In Section 3, we show the SS distributions obtained with the

*This work was supported by NIH Award Number 027164-00001

[1]Department of Mechanical Engineering, Massachusetts Institute of Technology, 77 Massachusetts Avenue, Cambridge, MA 02139. Emails: (sbruno,malirdwi,ddv)@mit.edu

[2]Department of Electrical and Computer Engineering and Department of Bioengineering, Northeastern University, 805 Columbus Ave, Boston, MA 02115, USA. Email: e.sontag@northeastern.edu

computational and analytical methods. Then, in Section 4 we describe and compare the results obtained through OL control and through CL control. Conclusive remarks are presented in Section 5.

II. A DETERMINISTIC MODEL OF THE PL GRN

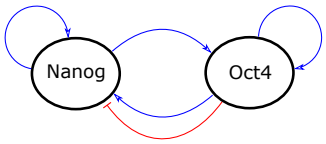

Figure 1: A two-node pluripotency gene regulatory network (PL GRN). Network model as taken from [1].

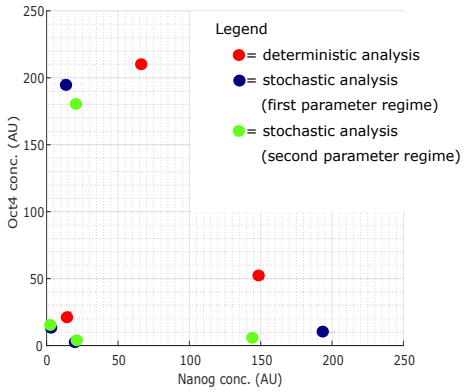

Figure 2: Comparison between location of stable SSs of the deterministic model and position of peaks of the SS probability distribution of the stochastic model. For the deterministic model, stable SSs of system in equations (1) are obtained as in [1]. For the stochastic model, the set of chemical reactions in Table I are simulated with parameter values given in Table II using the Gillespie algorithm [22].

The PL GRN proposed by Boyer et al. [19] is formed by three master TFs: Oct4, Nanog, and Sox2, which activate each other while self activating [4], [20]. Under the assumption of a sufficiently large number of molecules and sufficiently large volume, an ODE model was proposed in [1]. This PL GRN model is characterized by two nodes in which Oct4 and Sox2 were lumped together since they heterodimerize. Furthermore, to account for the observation that higher Oct4 concentration leads to lower Nanog concentration, a repressive term (from Oct4 to Nanog) was added. A diagram of the PL GRN model is shown in Fig. 1. In particular, letting x_1 represent [Nanog] and x_2 [Oct4], the ODE model is given as follows ([1]):

$$\dot{x_1} = H_1(x) - \gamma_1 x_1, \;\; \dot{x_2} = H_2(x) - \gamma_2 x_2, \qquad (1)$$

where the first term of each equation is a Hill function ([21]) capturing all the transcriptional regulations, and the terms $-\gamma_i x_i$ represent dilution and degradation. With the parameter values and specific form of the Hill functions taken from [1], this system displays three stable SSs, each characterized by specific levels of TFs: the PL stem cell, the trophectoderm (TR) and primitive endoderm (PE) cells (differentiated cells). The three SSs are shown in red in Fig. 2.

III. STOCHASTIC MODEL OF THE PL GRN

A deterministic model is not always sufficiently representative of a biomolecular system because the cell differentiation dynamics is often driven by noise, due, in part, to the combination of low molecular counts (e.g. one or two copies of a TF's gene) and slow promoter kinetics [15]. That is, binding of TFs with DNA in mammalian cells can be very slow due to the poor accessibility of gene promoters given that it is tightly wrapped around nucleosomes [23], [24].

Therefore, we consider the constituent reactions of the two-node PL GRN as given in [1] and create a CME model for this system. The reactions for the whole PL GRN (the plant to be controlled) are collected in Table I with parameter values given in Table II and taken from [1]. In particular, 15 species are involved: the TFs N and O (Nanog and Oct4), the TF dimers N_2 and O_2, the corresponding mRNA species m_N and m_O and all the promoter-TF binding configurations. Specifically, we have the free TF DNA promoters D_N and D_O, the single-bound promoters D_{NO}, D_{ON}, D_{NN} and D_{OO} (defining D_{ij} as the i promoter bound by the dimer of species j), the double-bound promoters D_{NNO} and D_{ONO} (defining D_{ijz} as the single-bound promoter D_{ij} bound by the dimer of species k), and D_X, that is the N promoter D_{NO} additionally bound by O_2 and represents the transcriptionally inactive form of D_{NO} being repressed by O_2 [1]. Concerning the reactions involved, we have the dimerization (reactions 1, 13), the TFs binding and unbinding (2-5, 14-17), the TFs transcription (TX) (6-9, 18-21) and translation (TL) (10, 22), decay (11, 12, 23, 24) and the repression from Oct4 to Nanog (X).

In order to study the effects of stochasticity, we implement the reactions through the stochastic simulation algorithm (SSA) ([22]) for two parameter regimes. We first consider the limit of slow promoter kinetics (i.e., $d_1, ..., d_8 \ll \alpha_O^0, ...\alpha_O^3, \alpha_N^0, ...\alpha_N^3$, signifying that the reversibe binding dynamics is much slower than TX) and one copy number for each TF's gene (i.e., $D_{tot} = \sum_{i \in O,ON,OO,ONO} D_i = \sum_{i \in N,NO,NN,NNO,X} D_i = 1$). For this specific parameter regime, we also apply the analytical method proposed by [17] in order to gain further insight on the effect of the controller.

R_j	Reaction	Prop.Func.(a_j)
1f	$O + O \xrightarrow{a_O} O_2$	$a_{1f} = \frac{a_O O(O-1)}{2\Omega}$
1r	$O_2 \xrightarrow{d_O} O + O$	$a_{1r} = d_O O_2$
2f	$D_O + N_2 \xrightarrow{a_1} D_{ON}$	$a_{2f} = \frac{a_1 N_2 D_O}{\Omega}$
2r	$D_{ON} \xrightarrow{d_1} D_O + N_2$	$a_{2r} = d_1 D_{ON}$
3f	$D_O + O_2 \xrightarrow{a_2} D_{OO}$	$a_{3f} = \frac{a_2 O_2 D_O}{\Omega}$
3r	$D_{OO} \xrightarrow{d_2} D_O + O_2$	$a_{3r} = d_2 D_{OO}$
4f	$D_{ON} + O_2 \xrightarrow{a_3} D_{ONO}$	$a_{4f} = \frac{a_3 O_2 D_{ON}}{\Omega}$
4r	$D_{ONO} \xrightarrow{d_3} D_{ON} + O_2$	$a_{4r} = d_3 D_{ONO}$
5f	$D_{OO} + N_2 \xrightarrow{a_4} D_{ONO}$	$a_{5f} = \frac{a_4 N_2 D_{OO}}{\Omega}$
5r	$D_{ONO} \xrightarrow{d_4} D_{OO} + N_2$	$a_{5r} = d_4 D_{ONO}$
6	$D_O \xrightarrow{\alpha_O^0} D_O + m_O$	$a_6 = \alpha_O^0 D_O$
7	$D_{ON} \xrightarrow{\alpha_O^1} D_{ON} + m_O$	$a_7 = \alpha_O^1 D_{ON}$
8	$D_{OO} \xrightarrow{\alpha_O^2} D_{OO} + m_O$	$a_8 = \alpha_O^2 D_{OO}$
9	$D_{ONO} \xrightarrow{\alpha_O^3} D_{ONO} + m_O$	$a_9 = \alpha_O^3 D_{ONO}$
10	$m_O \xrightarrow{K_O} m_O + O$	$a_{10} = K_O m_O$
11	$m_O \xrightarrow{\delta_O} 0$	$a_{11} = \delta_O m_O$
12	$O \xrightarrow{\gamma_O} 0$	$a_{12} = \gamma_O O$
13f	$N + N \xrightarrow{a_N} N_2$	$a_{13f} = \frac{a_N N(N-1)}{2\Omega}$
13r	$N_2 \xrightarrow{d_N} N + N$	$a_{13r} = d_N N_2$
14f	$D_N + N_2 \xrightarrow{a_5} D_{NN}$	$a_{14f} = \frac{a_5 N_2 D_N}{\Omega}$
14r	$D_{NN} \xrightarrow{d_5} D_N + N_2$	$a_{14r} = d_5 D_{NN}$
15f	$D_N + O_2 \xrightarrow{a_6} D_{NO}$	$a_{15f} = \frac{a_6 O_2 D_N}{\Omega}$
15r	$D_{NO} \xrightarrow{d_6} D_N + O_2$	$a_{15r} = d_6 D_{NO}$
16f	$D_{NN} + O_2 \xrightarrow{a_7} D_{NNO}$	$a_{16f} = \frac{a_7 O_2 D_{NN}}{\Omega}$
16r	$D_{NNO} \xrightarrow{d_7} D_{NN} + O_2$	$a_{16r} = d_7 D_{NNO}$
17f	$D_{NO} + N_2 \xrightarrow{a_8} D_{NNO}$	$a_{17f} = \frac{a_8 N_2 D_{NO}}{\Omega}$
17r	$D_{NNO} \xrightarrow{d_8} D_{NO} + N_2$	$a_{17r} = d_8 D_{NNO}$
18	$D_N \xrightarrow{\alpha_N^0} D_N + m_N$	$a_{18} = \alpha_N^0 D_N$
19	$D_{NO} \xrightarrow{\alpha_N^1} D_{NO} + m_N$	$a_{19} = \alpha_N^1 D_{NO}$
20	$D_{NN} \xrightarrow{\alpha_N^2} D_{NN} + m_N$	$a_{20} = \alpha_N^2 D_{NN}$
21	$D_{NNO} \xrightarrow{\alpha_N^3} D_{NNO} + m_N$	$a_{21} = \alpha_N^3 D_{NNO}$
22	$m_N \xrightarrow{K_N} m_N + N$	$a_{22} = K_N m_N$
23	$m_N \xrightarrow{\delta_N} 0$	$a_{23} = \delta_N m_N$
24	$N \xrightarrow{\gamma_N} 0$	$a_{24} = \gamma_N N$
Xf	$D_{NO} + O_2 \xrightarrow{a_{inc}} D_X$	$a_{Xf} = \frac{a_{inc} O_2 D_{NO}}{\Omega}$
Xr	$D_X \xrightarrow{d_{inc}} D_{NO} + O_2$	$a_{Xr} = d_{inc} D_X$

Table I: Endogenous circuit reactions

Second, we computationally investigate the case in which the copy number for each TF's gene is 1 and the promoter kinetics is on the same time scale as TX (ie., $d_1, ..., d_8 \approx \alpha_O^0, ...\alpha_O^3, \alpha_N^0, ...\alpha_N^3$), which may be a more realistic assumption for certain applications [16].

A. Steady state probability distribution of uncontrolled PL GRN

To depict the stationary probability distribution of the PL GRN model, we run the SSA on the chemical reactions listed in Table I with parameter values given in Table II, considering a uniform distribution of initial concentrations in the state space (N, O). For all the other initial concentrations, we set, for each (N, O) pair, the corresponding equilibrium values [1]. The simulation results were used to build a 2D histogram, depicting for each (N, O) pair the fraction of simulations that resulted in that pair after the system transient response had

Parameter	Value (AU)	Parameter	Value (AU)
D_{cn}ideal	100	D_{co}ideal	100
D_{cn}real	5	D_{co}real	5
a_1-a_8,a_O,a_N	1*ϵ	d_1-d_8,d_O,d_N	100*ϵ
κ_O	1	κ_N	1
α_O^0	0.01872/Cn	α_N^0	0.12/Cn
α_O^1	0.0707/Cn	α_N^1	18.85/Cn
α_O^2	0.81/Cn	α_N^2	4.64/Cn
α_O^3	0.83/Cn	α_N^3	15.82/Cn
a_{inc}	0.01	d_{inc}	0.10
a_{sn}	0.01	a_{so}	0.01
d_{sn}	61	d_{so}	61
k_{sn}	61	k_{so}	61
δ_N	0.09	δ_O	0.17
γ_N	0.139	γ_O	0.046
β_N	0.05	β_O	0.05
$h_{N,1}$	19.23	$h_{O,1}$	0.89
$h_{N,2}$	6.7	$h_{O,2}$	6.7
Cn = Copy number	1	ϵ	$10^{-3}, 10^{-5}$

Table II: Parameters of the PL GRN and of the controller circuit.

extinguished.

For the slow promoter kinetic regime, we considered the parameter values listed in Table II (we set ϵ, that is the parameter through which we regulate the TFs binding and unbinding rates, equal to 10^{-5}) and the results are shown in Fig. 3. Under the slow promoter kinetic assumption, we can further derive the SS PDF analytically by using the results of [17], which we briefly summarize as follows. Let $Z(t) \in \mathbb{Z}_{\geq 0}^n$ be the vector of copy numbers of all the species in the network at time t and let $p_z(t) = \Pr[Z(t) = z]$ be the probability that $Z(t) = z$ for $z \in \mathbb{R}^n$. Let z_0, z_1,... be all the possible values z and $p(t) = [p_{z_0}, p_{z_1}, ..]^T$, then the CME can be written as

$$\dot{p} = \Lambda p(t), \tag{2}$$

where Λ is the infinitisimal generator of the Markov chain which describes the stochastic evolution of species' counts [17]. Letting R_j represent the propensity function related to the reaction R_j and γ_j the stochiometry vector related to the reaction R_j ([21]), each element of Λ can be defined as:

$$\lambda_{x\tilde{x}} := \begin{cases} R_j(x) & \text{if } \exists j : \tilde{x} = x - \gamma_j \\ -\sum_{j=1}^m R_j(z) & \text{if } \tilde{x} = x \\ 0 & \text{otherwise,} \end{cases} \tag{3}$$

In the GRN we can split $Z(t)$ into "gene process" $D(t)$, i.e., the TFs binding/unbinding reactions, and "protein process" $X(t)$, i.e., the protein production (that is the TX and TL lumped together), dimerization and decay, and then we can decompose the probability distribution vector correspondingly. Being $p_{dx}(t) = \Pr[X(t) = x, D(t) = d]$ the joint probability distribu-

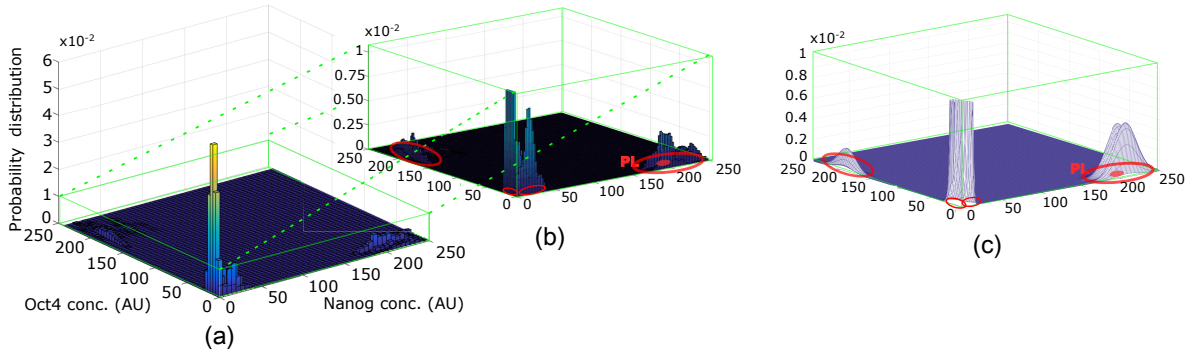

Figure 3: Steady state probability distribution of the uncontrolled PL GRN in the slow promoter kinetic regime. (a) and **(b)** show the distribution as obtained from Gillespie simulation of the system of reactions listed in Table I with the parameter values given in Table II. **(c)** SS probability distribution analytically computed through (8). We indicate with PL the location of the PL peak of the system without control input.

tion of X and D, we can define the vector $p_d(t) = [p_{dx_0}(t), p_{dx_1}(t), ...]^T$ in which we collect, for a certain d, the probabilities of all the possible x [17]. Hence, using the notation above and defining L as the total number of all the possible d, we can decompose the CME (2) as

$$\dot{p}(t) = \Lambda p(t) = \left(\tilde{\Lambda} + \varepsilon\hat{\Lambda}\right) p(t), \tag{4}$$

where

$$\tilde{\Lambda} = \begin{bmatrix} \Lambda_0 & & \\ & \ddots & \\ & & \Lambda_{L-1} \end{bmatrix}, \text{ and } p(t) = \begin{bmatrix} p_0(t) \\ \vdots \\ p_{L-1}(t) \end{bmatrix} \tag{5}$$

The slow matrix $\hat{\Lambda}$ contains the propensity functions from the gene processes, while the fast matrix $\tilde{\Lambda}$ contains the propensity functions of the protein processes. Each of the submatrices $\Lambda_0, ..., \Lambda_{L-1}$ of $\tilde{\Lambda}$ in (5) can be interpreted as an infinitesimal generator for the network conditioned on a certain promoter configuration d, i.e., Λ_i is the infinitesimal generator for the Markov chain conditioned on $D(t) = i$. Applying singular perturbation theory to the CME (i.e., setting ϵ equal to zero) [18], the overall SS probability distribution can be evaluated with the following formula:

$$\pi(x, d) = \sum_{d=0}^{L-1} \rho_d \pi_{X|d}(x, d), \tag{6}$$

where ρ_d is a weighting coefficient that represents the fraction of time that the system will spend in the configuration d and $\pi_{X|d}(x, d)$ is the stationary distribution conditioned on d. $\pi_{X|d}(x, d)$ can be expressed as Poisson distribution ([17]):

$$\pi_{X|d}(x, d) := \mathbf{P}(x, a) := \frac{a^x}{x!} e^{-a}, \tag{7}$$

where a is the mean value of the distribution, defined as the ratio between the protein production rate constant (i.e., the product between the TX rate constant and the TL rate constant, divided by the mRNA degradation rate constant) and the protein degradation rate constant. Hence, the overall stationary distribution is a linear combination of Poisson distributions. ρ_d can be evaluated as the principal normalized eigenvector of the matrix Λ_r, in which any (d', d) entry represents the probability of transition from the configuration d' to configuration d and can be computed through an algorithm given in [17].

In our case, the gene reactions are reactions 2-5, 14-17, X listed in Table I, protein reactions are all the others of Table I (considering TX and TL reactions lumped together as protein production reactions) and we can describe the promoter configurations with two processes $D_N(t)$ (i.e., N, NO, NN, NNO, X) and $D_O(t)$ (i.e., O, ON, OO, ONO), which are indexed as $0, 1, 2, 3, 4$ and $0, 1, 2, 3$, respectively. Considering all the possible promoter configurations, formula (6) becomes:

$$\pi = \sum_{i=0}^{4} \sum_{j=0}^{3} \rho_{ij} \mathbf{P}(N, O; \frac{K_N^i}{\gamma_N}, \frac{K_O^j}{\gamma_O}), \tag{8}$$

where ρ_{ij} represents a weighting coefficient, $K_N^i = \frac{\alpha_N^i K_N}{\delta_N}$ and $K_O^j = \frac{\alpha_O^j K_O}{\delta_O}$ represent the gene expression rates of N and O, in which, referring to the Table I, α_N^i and α_O^j are the TX rates of m_N and m_O, K_N and K_O represent the TL rates of N and O, and δ_N and δ_O are the degradation rate constants of m_N and m_O, respectively. Furthermore, γ_N and γ_O represent the degradation rate constants of N and O and, as a consequence, the ratios $\frac{K_N^i}{\gamma_N}$ and $\frac{K_O^j}{\gamma_O}$ represent the SS protein level resulting from each promoter configuration.

Fig. 3(b)-(c) show good agreement between the SS distributions computed numerically and analytically: there are four major modes (local maximum of the PDF): one in the "high N - low O" region, one in the "low N - high O" region and two in the "low N - low O" region.

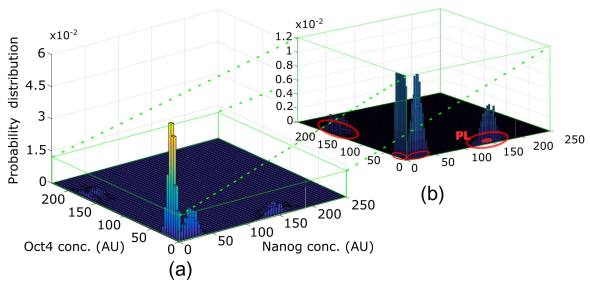

Figure 4: Steady state probability distribution of the uncontrolled PL GRN in the comparable time scale regime. **(a)** and **(b)** show the distribution as obtained from Gillespie simulation of the system of reactions listed in Table I with the parameter values given in Table II.

Concerning the comparable time scale parameter regime, we considered the parameter values listed in Table II (in particular, we set ϵ equal to 10^{-3}) and the results are shown in Fig. 4. Comparison between the results of the two parameter regimes, shown in Fig. 3 and 4, highlights a difference in the position of the mode in the "high N - low O" region: in the slow promoter kinetic regime it is characterized by a higher value of Nanog ($\approx$190 AU) compared to the PL state in the comparable time scale case ($\approx$140 AU).

Referring to Fig.2, it is possible to notice that, compared to the deterministic results, in both analyzed parameter regimes the number of the major modes (four) is higher than the number of the stable SSs in the deterministic model (three). In particular:

- as in the deterministic analysis, there is a mode in the "low N - high O" region corresponding to the PE state and a mode in the "high N - low O" region corresponding to the PL state. However, their position is slightly changed compared to the stable SS obtained through the deterministic study.
- differently from the deterministic analysis, in the "low N - low O" region there are two modes very close to each other, instead of one stable SS.

IV. Reprogramming approaches

In this section, we compare the SS probability distribution of the controlled PL GRN with OL and CL control. The objective of the control is to obtain a unimodal SS probability distribution with peak sufficiently close to the PL state.

A. OL control: prefixed overexpression reprogramming approach

In an OL control, i.e., the approach used by the standard iPSC reprogramming protocol, the production rate of key TFs (Nanog and Oct4 for our model) is artificially increased [3]. This reprogramming approach can be realized by the introduction of the additional reactions listed in Table III to the reaction system shown in Table I [3].

R(j)	Reaction	Prop.Func.(a_j)	R(j)	Reaction	Prop.Func.(a_j)
25	$0 \xrightarrow{u_2} O$	$a_{1f} = u_2$	26	$0 \xrightarrow{u_1} N$	$a_{13f} = u_1$

Table III: OL control reactions

In order to determine the outcome of this strategy, we again implemented the reactions through the Gillespie algorithm with increasing values of u_1 and u_2. Results under the slow promoter kinetic assumption are shown in Fig. 5. As u_1 and u_2 increase, the stationary distribution "shifts" towards higher copy number of the overexpressed TF and the peak of the mode corresponding to the maximal expression becomes higher to the detriment of the peak height of the modes characterized by a lower protein expression. In more detail, increasing u_2, the stationary distribution shifts towards higher copy number of Oct4, thus the system cannot be reprogrammed to PL state because it is characterized by a lower copy number of Oct4. Increasing u_1, the stationary distribution shifts towards higher copy number of Nanog and then, in theory, we could obtain a unimodal distribution near PL, which is characterized by Nanog $\approx$ 190 AU. However, gradually varying the inputs, we were unable to find a unimodal stationary PDF. For example, the case where $u_1 = 1.5$, shown in Fig. 5(a), is still multimodal. Then, for higher values of u_1, the distribution will continue shifting and, even if we obtained a unimodal distribution, the unique mode would be far from PL. From these findings we can conclude that we do not obtain a unimodal distribution near PL for prefixed overexpression of either one or both TFs.

In order to gain insight on the effects of prefixed overexpression on the shape of the SS probability distribution, we explicitly write this distribution using the method explained in Section 3. Specifically, prefixed overexpression implies that the protein production rate constants K_N^i and K_O^j in Eq. (8) should be increased by adding u_1 and u_2, respectively. Hence, formula (8) becomes

$$\pi = \sum_{i=0}^{4}\sum_{j=0}^{3} \rho_{ij}^{u} \mathbf{P}(N, O; \frac{(K_N^i + u_1)}{\gamma_N}, \frac{(K_O^j + u_2)}{\gamma_O}), \quad (9)$$

where $\{\rho_{ij}^u\}$ are the weighting coefficients with the modified TFs production rates. Analyzing the Poisson distributions, the modified constants $K_N^i + u_1$ and $K_O^j + u_2$, higher than K_N^i and K_O^j in Eq. (8), lead to higher values of the Poisson distributions' mean and then to a SS probability distribution "shifted" towards higher copy number. Furthermore, Fig. 5(b) illustrates that, as u_1 or u_2 grow, the ρ_{ij}^u corresponding to the promoter's configuration leading to maximal TF expression becomes larger, while all the other ρ_{ij}^u become smaller. This

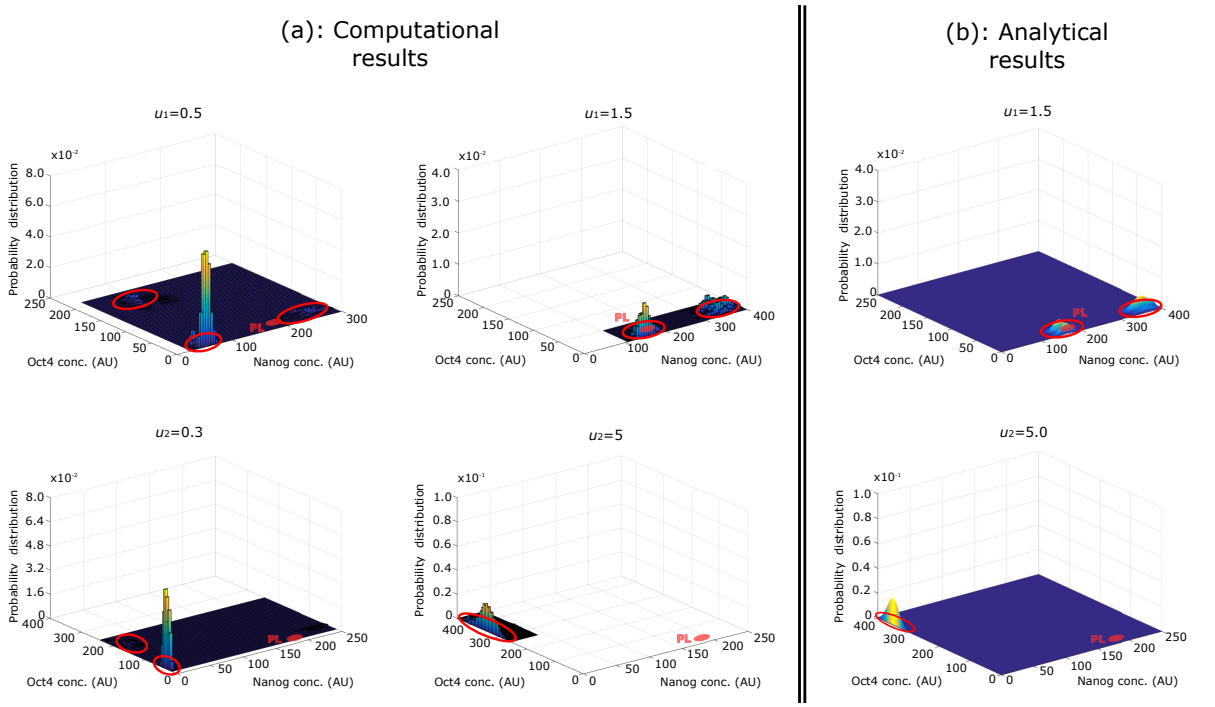

Figure 5: Constant overexpression results in the slow promoter kinetics regime:(a) shows the distribution as obtained from Gillespie simulation of the system of reactions listed in Tables I and III with the parameter values given in Table II. **(b)** is the steady state probability distribution analytically computed through Formula (9). The values of u_1 and u_2 that we have set are written on the top of each graph.

implies that we do not achive a unimodal PDF near PL state, consistently with the results obtained through SSA.

Concerning the comparable time scale regime, the obtained results show accordance to those obtained with slow promoter kinetics.

B. CL control: feedback overexpression through a synthetic genetic controller circuit

The absence of guarantees of success with the OL control approach led a novel CL feedback control reprogramming approach [1]. Within this approach, the input is adjusted based on the difference between the current state and the desired one, as encoded by the TFs concentrations. Referring to the deterministic model in equations (1), this feedback overexpression translates into an input of the form $u_i = G_i(m_i^* - m_i)$ where G_i is a non-negative constant and m_i^* is the mRNA desired value (i.e., the concentration of the TF's mRNA found in the PL state). Letting x_1 represent [Nanog] and x_2 [Oct4], the model becomes

$$\begin{aligned} \dot{m}_i &= H_i(x) - \delta_i m_i + G_i(m_i^* - m_i), \\ \dot{x}_i &= k_i m_i - \gamma_i x_i, \end{aligned} \tag{10}$$

in which $i = 1, 2$. If G_i is sufficiently large (that, in practice, means infecting the cells with sufficiently large virus copy number), $\dot{m}_i \approx G_i(m_i^* - m_i)$ and, at SS, $m_i = m_i^*$: the unique SS of the system will be the desired one, that is $\frac{k_i m_i^*}{\gamma_i} =: x_i^*$ [1]. To implement this feedback strategy, a genetic circuit regulating the overexpression and degradation of the m_i of the species x_i simultaneously has been proposed [1]. Fig. 6 shows the implementation of this circuit: the overexpression is obtained through inducible TX of the TF x_i through inducer $I_{i,1}$ and the m_i degradation is obtained by using a small interfering RNA (siRNA) s_i, RNA molecules that bind and degrade mRNA [25]. The s_i transcript is induced by inducer $I_{i,2}$ on the same DNA D_{Ci}.

Considering a one-step enzymatic reaction for the m_i degradation ($0 \xrightarrow{D_{Ci}h_{i,2}(I_{i,2})} s_i; m_i + s_i \xrightarrow{k_{si}} s_i; s_i \xrightarrow{\beta_i} 0$, where k_{si} is the catalytic rate constant and β_i is the diluition rate constant), the ODE model of our system becomes

$$\begin{aligned} \dot{s}_i &= D_{Ci}h_{i,2}(I_{i,2}) - \beta_i s_i \\ \dot{m}_i &= H_i(x) - \delta_i m_i + D_{Ci}h_{i,1}(I_{i,1}) - k_{si}s_i m_i, \\ \dot{x}_i &= k_i m_i - \gamma_i x_i. \end{aligned} \tag{11}$$

When s_i reaches the equilibrium ($s_i^* = \frac{D_{Ci}h_{i,2}(I_{i,2})}{\beta_i}$), the ODE describing the evolution of m_i becomes $\dot{m}_i = H_i(x) - \delta_i m_i + D_{Ci}h_{i,1}(I_{i,1}) - k_{si}s_i^* m_i$ and, defining $G_i = \frac{D_{Ci}k_{si}h_{i,2}(I_{i,2})}{\beta_i}$ and $m_i^* = \frac{\beta_i h_{i,1}(I_{i,1})}{k_{si}h_{i,2}(I_{i,2})}$, the system can be re-written as follows:

$$\begin{aligned} \dot{m}_i &= H_i(x) - \delta_i m_i + G_i(m_i^* - m_i), \\ \dot{x}_i &= k_i m_i - \gamma_i x_i. \end{aligned} \tag{12}$$

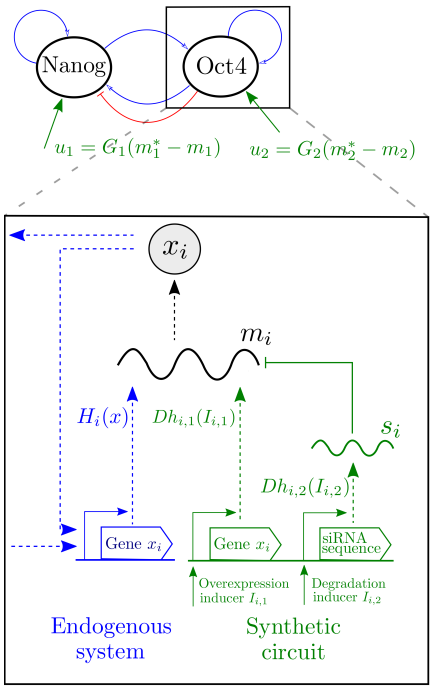

Figure 6: CL control reprogramming approach implementation. The overexpression is regulated by the inducer $I_{i,1}$ and the siRNA-based degradation is regulated by $I_{i,2}$. The endogenous mRNA is produced with a rate given by the Hill function $H_i(x)$. The synthetic mRNA is produced with a rate equal to $Dh_{i,1}(I_{i,1})$ where D is the DNA concentration and $h_{i,1}$ is the function representing how the inducers activate the genes [1].

R(j)	Reaction	Prop.Func.(a_j)
25	$D_{CO} \xrightarrow{h(I_{O,1})} D_{CO} + m_O$	$a_{25} = h(I_{O,1})D_{CO}$
26	$D_{CO} \xrightarrow{h(I_{O,2})} D_{CO} + s_O$	$a_{26} = h(I_{O,2})D_{CO}$
27f	$m_O + s_O \xrightarrow{a_{SO}} c_O$	$a_{27f} = \frac{a_{SO} m_O s_O}{\Omega}$
27r	$c_O \xrightarrow{d_{SO}} m_O + s_O$	$a_{27r} = d_{SO} c_O$
28	$c_O \xrightarrow{k_{SO}} s_O$	$a_{28} = k_{SO} c_O$
29	$s_O \xrightarrow{\beta_O} 0$	$a_{29} = \beta_O s_O$
30	$C_O \xrightarrow{\beta_O} 0$	$a_{30} = \beta_O C_O$
31	$D_{CN} \xrightarrow{h(I_{N,1})} D_{CN} + m_N$	$a_{31} = h(I_{N,1}) D_{cn}$
32	$D_{CN} \xrightarrow{h(I_{N,2})} D_{CN} + s_N$	$a_{32} = h(I_{N,2}) D_{cn}$
33f	$m_N + s_N \xrightarrow{a_{SN}} c_N$	$a_{33f} = \frac{a_{SN} m_N s_N}{\Omega}$
33r	$c_N \xrightarrow{d_{SN}} m_N + s_N$	$a_{33r} = d_{SN} c_N$
34	$c_N \xrightarrow{k_{SN}} s_N$	$a_{34} = k_{SN} c_N$
35	$s_N \xrightarrow{\beta_N} 0$	$a_{35} = \beta_N s_N$
36	$C_N \xrightarrow{\beta_N} 0$	$a_{36} = \beta_N C_N$

Table IV: CL control reactions

As described above, if G_i is large enough, the unique SS is the desired one. It is possible to notice that the gain G_i is directly proportional to D_{Ci}, and $I_{i,1}$ is tuned on the basis of the stable SS (N^*, O^*) that we want to obtain with the controller. As it is explained in detail in [1], this still holds if we have a more realistic two-step enzymatic reaction for the m_i degradation. Then, the reactions to add to the ones in Table I to form the CL system are listed in Table IV [1]. In particular, in the two-step enzymatic reaction for the mRNA degradation (reactions 27, 28, 33, 34 in Table IV), c_N and c_O are the intermediate complexes generated during the degradation, and D_{CN} and D_{CO} represent the DNA where the synthetic circuit is encoded.

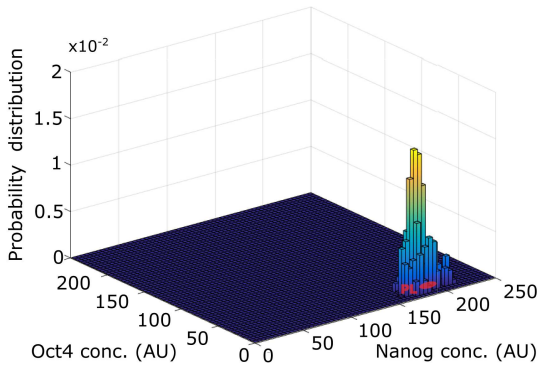

Figure 7: Feedback overexpression results in the slow promoter kinetic regime. The distribution is obtained from SSA simulation of the system of reactions listed in Tables I and IV with the parameter values given in Table II.

We first analyzed the performance of the controller in the slow promoter kinetic parameter regime: the SSA was implemented with parameters given in Table II and the results are shown in Fig. 7. They highlight that the feedback overexpression approach allows us to obtain a unimodal PDF for the CL system with the peak near the desired state (i.e., PL), meeting the prefixed objective.

The reason why this feedback law is theoretically guaranteed to result in a unimodal distribution for sufficiently large gain G_i can be explained by analytically calculating the SS PDF with the formula (8), introduced in Section 3, for the CL approach. To provide a simple formula that can be easily inspected, we consider enhanced degradation of the protein (instead of the mRNA) and we assume that it occurs through a one-step enzymatic reaction. Then, the formula (8) for the CL feedback system is modified by adding the following reactions:

$$0 \xrightarrow{G_2 O^*} O, 0 \xrightarrow{D_{C2} h_{2,2}(I_{2,2})} S_2; S_2 + O \xrightarrow{k_{s2}} S_2, S_2 \xrightarrow{\beta_2} 0,$$

$$0 \xrightarrow{G_1 N^*} N, 0 \xrightarrow{D_{C1} h_{1,2}(I_{1,2})} S_1; S_1 + N \xrightarrow{k_{S1}} S_1, S_1 \xrightarrow{\beta_1} 0,$$

where G_i (with $i = 1, 2$) is defined as $\frac{D_{Ci} k_{si} h_{i,2}(I_{i,2})}{\beta_i}$ and S_1 and S_2 are the proteases that degradate N and O, respectively. These reactions are equivalent to the following ones:

$$0 \xrightarrow{G_2 O^*} O, O \xrightarrow{G_2} 0; 0 \xrightarrow{G_1 N^*} N, N \xrightarrow{G_1} 0,$$

that represent the overexpression and degradation of O and N applied through this control strategy. It means that the TFs espression rates K_N^i and K_O^j increase by G_1N^* and G_2O^*, and the degradation rates γ_N and γ_O increase by G_1 and G_2, respectively. Hence, Eq. (8) takes the form

$$\pi = \sum_{i=0}^{4}\sum_{j=0}^{3}\rho_{ij}\mathbf{P}(N, O; \frac{(K_N^i + G_1N^*)}{\gamma_N + G_1}, \frac{(K_O^j + G_2O^*)}{\gamma_O + G_2}), \tag{13}$$

in which, when G_1 and G_2 are sufficiently large, we obtain that $\frac{(K_N^i+G_1N^*)}{\gamma_N+G_1} \approx N^*$ and $\frac{(K_O^j+G_2O^*)}{\gamma_O+G_2} \approx O^*$. As a consequence, all the peaks coincide and are located at the desired location (N^*, O^*). The computational results, shown in Fig. 7, are in agreement with these analytical results. In fact in both cases a feedback overexpression leads to a stationary distribution characterized by a unique mode (i.e., the target mode).Then, these results demonstrate that the feedback overexpression control law adopted in [1] performs as desired even in the presence of significant stochastic effects, such as those deriving from slow promoter kinetcs, small volume and low copy number.

Concerning the comparable time scale parameter regime, the obtained results are very similar to the ones obtained for the slow promoter kinetics regime.

V. Conclusions

In this work, a stochastic model for iPSC reprogramming has been considered through the CME. This model takes into account the stochastic effects on both the PL GRN and the feedback controller circuit, as stemming from low molecule counts and slow promoter kinetics. Specifically, we conducted numerical simulations for the CME of both OL and CL systems through the SSA. Two parameter regimes were analyzed and simulation outputs compared. The first regime (i.e., the reversible binding dynamics is much slower than TX), for which analytical results are also possible and demonstrate that, despite the controller is stochastic and the PL GRN operates in regimes where stochastic behavior cannot be neglected, the CL approach still works, allowing us to obtain a unimodal PDF near PL. For the second regime where the reversible binding dynamics is comparable to TX, only computational simulations were performed, which show accordance with the results of the first regime. Future work will address the experimental implementation of the controller.

References

[1] D. D. Vecchio, H. Abdallah, Y. Qian, and J. J. Collins, "A blueprint for a synthetic genetic feedback controller to reprogram cell fate," *Cell systems*, vol. 4 1, pp. 109–120.e11, 2017.

[2] G. Chu, "Embryonic stem-cell research and the moral status of embryos," *Internal Medicine Journal*, vol. 33, no. 11, pp. 530–531.

[3] K. Takahashi and S. Yamanaka, "Induction of pluripotent stem cells from mouse embryonic and adult fibroblast cultures by defined factors," *Cell*, 2006.

[4] T. W. Theunissen and R. Jaenisch, "Molecular control of induced pluripotency," *Cell Stem Cell*, 2014.

[5] B. C. Heng and M. Fussenegger, *Integration-Free Reprogramming of Human Somatic Cells to Induced Pluripotent Stem Cells (iPSCs) Without Viral Vectors, Recombinant DNA, and Genetic Modification*. New York, NY: Springer New York, 2014, pp. 75–94.

[6] N. Malik and M. S. Rao, "A review of the methods for human ipsc derivation," *Methods in molecular biology*, vol. 997, pp. 23–33, 2013.

[7] T. M. Schlaeger and L. Daheron, "A comparison of non-integrating reprogramming methods," *Biotechnology*, vol. 33, no. 1, pp. 58–63, 2015.

[8] P. C. Faucon and et al., "Gene networks of fully connected triads with complete auto-activation enable multistability and stepwise stochastic transitions," *PLoS ONE*, vol. 9, 2014.

[9] H. Smith, *Monotone Dynamical Systems*. American Mathematical Society, 1995.

[10] H. Niwa, "How is pluripotency determined and maintained?" *Development*, vol. 134, no. 4, pp. 635–646, 2007.

[11] E. Warlich, J. Kuehle, T. Cantz, M. H. Brugman, T. Maetzig, M. Galla, A. A. Filipczyk, S. Halle, H. Klump, H. R. Schöler, C. Baum, T. Schroeder, and A. Schambach, "Lentiviral vector design and imaging approaches to visualize the early stages of cellular reprogramming," *Molecular Therapy*, vol. 19, no. 4, pp. 782 – 789, 2011.

[12] H. H. McAdams and A. Arkin, "Stochastic mechanisms in gene expression," *Proceedings of the National Academy of Sciences*, vol. 94, no. 3, pp. 814–819, 1997.

[13] M. B. Elowitz, A. J. Levine, E. D. Siggia, and P. S. Swain, "Stochastic gene expression in a single cell," *Science*, vol. 297, no. 5584, pp. 1183–1186, 2002.

[14] J. M. Raser and E. K. O'Shea, "Control of stochasticity in eukaryotic gene expression," *Science*, vol. 304, no. 5678, pp. 1811–1814, 2004.

[15] G. Balázsi, A. van Oudenaarden, and J. J. Collins, "Cellular decision making and biological noise: From microbes to mammals," *Cell*, vol. 144, pp. 910–925, 2011.

[16] A. M. Walczak, J. N. Onuchic, and P. G. Wolynes, "Absolute rate theories of epigenetic stability," *Proceedings of the National Academy of Sciences of the United States of America*, vol. 102(52), p. 18926–18931, 2005.

[17] M. A. Al-Radhawi, D. D. Vecchio, and E. D. Sontag, "Multi-modality in gene regulatory networks with slow promoter kinetics," *PLOS Computational Biology*, vol. 15, no. 2, pp.1–27, 2019.

[18] S. Campbell and N. Rose, "Singular perturbation of autonomous linear systems," *SIAM Journal on Mathematical Analysis*, vol. 10, no. 3, pp. 542–551, 1979.

[19] L. A. Boyer, T. I. Lee, and M. F. C. et al., "Core transcriptional regulatory circuitry in human embryonic stem cells," *Cell*, vol. 122, pp. 947–956, 2005.

[20] R. Jaenisch and R. Young, "Stem cells, the molecular circuitry of pluripotency and nuclear reprogramming," *Cell*, vol. 132, pp. 567–582, 2008.

[21] D. D. Vecchio and R. M. Murray, *Biomolecular feedback systems*. Priceton University Press, 2014.

[22] D. T. Gillespie, "Stochastic simulation of chemical kinetics," *Annual Review of Physical Chemistry*, vol. 58, no. 1, pp. 35–55, 2007, pMID: 17037977.

[23] D. Allis, M.-L. Caparros, T. Jenuwein, and D. Reinberg, *Epigenetics*. CSH Press, 2015.

[24] T. Kouzarides, "Chromatin modifications and their function," *Cell*, vol. 128, no. 4, pp. 693–705, 2007.

[25] R. W. Carthew and E. J. Sontheimer, "Origins and mechanisms of mirnas and sirnas," *Cell*, vol. 136, no. 4, pp. 642 – 655, 2009.